# Diffusion in tight confinement: A lattice-gas cellular automaton approach. II. Transport properties

Pierfranco Demontis,[a] Federico G. Pazzona, and Giuseppe B. Suffritti
*Dipartimento di Chimica, Università degli Studi di Sassari, and Consorzio Interuniversitario Nazionale per la Scienza e Tecnologia dei Materiali (INSTM), Unità di Ricerca di Sassari, via Vienna, 2 I-07100 Sassari, Italy*

(Received 20 September 2006; accepted 9 March 2007; published online 17 May 2007)

In this second paper the authors study the transport properties of the lattice-gas cellular automaton presented in Paper I [J. Chem. Phys. **126**, 194709 (2007)] to model adsorption and dynamics of particles in a lattice of confining cells. Their work shows how a surprisingly simple parallel rule applied to a static network of cells joined by links set in space and time can generate a wide range of dynamical behaviors. In their model the cells are the elementary constituent objects of the network. They are a portion of space structured in sites which are energetically different. Each cell can accommodate a given maximum number of particles, and each pair of neighboring cells can exchange at most one particle at a time. The predictions of the model are in qualitative agreement with both experimental observations and molecular dynamics simulation results. © *2007 American Institute of Physics*. [DOI: 10.1063/1.2721547]

## I. INTRODUCTION

Molecular motions in microporous materials cover a wide range of time scales: from bond vibrations at the femtosecond level to long-range diffusion at the microsecond or longer time scale depending on the specific conditions at which the phenomenon occurs.[1] Theoretically, phenomena with the fastest motions are studied by different methods, including first principles molecular dynamics[2] and classical molecular dynamics simulations.[3] These studies provide insight into the atomistic structure and interactions with the adsorbed molecules of the microporous framework. Other events, at slower time scales, such as ionic exchange or long-range diffusion are rarely suitable for studies with current classical molecular dynamics simulations as they span scales that are at least of an order of magnitude larger than the largest studies to date (hundreds of nanoseconds).[4] The investigation of these phenomena, even using models based on simple effective pairwise atom-atom potentials are still too computationally costly. Because most of the practical applications of these materials involve shape selective catalysis and separation processes, a field where the transport properties of adsorbed molecules play a central role, a question arises: what are the fundamental interactions that control the dependence of diffusion in microporous materials and can they be represented in a coarse grained fashion able to reproduce the main feature of the transport phenomena on very long time scale at very long distances? This motivates the search for a further simplification of the atomistic models of micropores, to reach a simpler description of the effective interactions such that they can be easily computed and at the same time able to capture the essential features of the real physical systems.[5–8] In the paper immediately preceding, denoted as Paper I, we describe in detail a lattice-gas cellular automaton (LGCA) able to model the properties of species bounded to an adsorbent's surface mainly focusing on the structural equilibrium properties of the model. In the following article we report the results concerning the dynamical properties that can be studied from the model. In short, our LGCA represents the connected channels and cages of a real microporous material as a lattice of communicating cells that can contain and exchange a fixed number of guest molecules. Each cell has the unit size λ and an appropriate number of energetically different adsorption sites: exit sites available to particle transfer and inner sites not available. This, along with the instantaneous number of molecules inside, determines the number of accessible states in each cell. In each cell the actual dynamic state (including its tendency to particle transfer) will be determined by the energies of its occupied sites according to a local Monte Carlo sampling scheme on the allowed states. In a previous paper[9] we have shown that a properly designed LGCA captures the essential physics of molecules confined to porous solids. The remainder of this paper is organized as follows: in Sec. II we report the results of the simulations, while in Sec. III we conclude by summarizing the present results and by remarking on the applicability of our approach for modeling other host-guest diffusion systems.

## II. RESULTS OF THE SIMULATIONS

We mapped on our LGCA model an Linde Type A (LTA) zeolite, the ZK4, a framework which satisfies the topology requirements of the model illustrated here.[10] This system consists in a simple cubic lattice of nearly spherical cavities with an internal radius of ~5.7 Å connected to six neighboring cavities by nearly circular windows of ~4.2 Å in diameter. We assume that each cavity can host a maximum of $K=16$ particles. These cavities are represented in our model by

[a]Author to whom correspondence should be addressed. Electronic mail: demontis@uniss.it

 

means of cells, each containing $\nu=6$ exit sites with adsorption
energy $-\varepsilon_{ex}$, which are available to particle transfers, and $K-\nu$ inner sites with adsorption energy $-\varepsilon_{in}$, which are not available to such transfers. Where not explicitly indicated, in this work all the simulations were performed on a cubic grid of $16^3$ cells. In this case study we assigned the same (dimensioned) values of site energies and temperatures as those employed by Bhide and Yashonath in their lattice-gas model study[11,12] in order to compare directly with their work our diffusivity curves. Therefore we set the energy parameters as $\varepsilon_{ex}=10$ kJ/mol and $\varepsilon_{in}=20$ kJ/mol. If not specified, we set the coefficient $\kappa_0$ of the propagation probability, which rules the frequency of intercell transfers [see Eq. (14) of Paper I for further details], as $\kappa_0=1$.

In each computer simulation, starting from a random distribution of particles, after 20 000 time steps of equilibration we observed the evolution of the system during a time interval ranging from $10^5$ to $10^8$ time steps, depending on the statistical accuracy required to compute the averages of interest. The data at temperature $T\to\infty$ are obtained from simulations with $\varepsilon_{ex}=\varepsilon_{in}$.

### A. Diffusion coefficients

In our simulations we computed the different diffusivities which are of most common interest in the study of the intercell migration in microporous systems.

The self-diffusion coefficient, which measures the diffusive motion of a single particle, can be computed from its mean-squared displacement at long times through

$$D_s=\frac{1}{2d}\lim_{t\to\infty}\frac{\mathrm{d}}{\mathrm{d}t}\langle[\mathbf{r}_i(t)-\mathbf{r}_i(0)]^2\rangle, \tag{1}$$

where $\mathbf{r}_i(t)$ is the position of a tagged particle (i.e., the cell it occupies) at time $t$, and $d$ is the dimensionality of the lattice.

The single-particle random walk is ideal (i.e., Markovian) if the probability of a particle to migrate from a cell to a neighboring one is independent of the previous history of the particle. In such a case, this probability equals $1/\tau_{mrt}$, where $\tau_{mrt}$ is the mean residence time (in units of time steps) of a particle inside a cell. We indicate the diffusivity associated to such a random walk as the ideal diffusivity $D_0$

$$D_0=\frac{\lambda^2}{\tau}\frac{1}{2d\tau_{mrt}}, \tag{2}$$

where $\lambda$ is the distance between two neighboring cells, and $\tau$ is the duration of a time step. Introducing $\langle n\rangle$ as the loading (average number of particles per cell), $\rho_{ex}$ as the relative particle density per exit site, and $\kappa_0$ and $A$ as fixed kinetic parameters (see Paper I and our previous work[9] for details about the calculation of these quantities), one obtains the following general expression for $D_0$:

$$D_0=\frac{\lambda^2}{\tau}\frac{1}{2d}\frac{\nu\rho_{ex}}{\langle n\rangle}(1-\rho_{ex})\kappa_0 A e^{-\beta\varepsilon_{ex}}, \tag{3}$$

where $\beta=1/k_BT$, with $k_B$ the Boltzmann constant. Details about the calculation of $D_0$ can be found in the Appendix.

If averaging over a long trajectory $D_s$ is found to converge to $D_0$, then the particle migration is unaffected by memory effects.

The collective diffusivity $D_c$ (often used in the zeolite literature)[13] measures the diffusive motion of the collective coordinate $\Sigma_{i=1}^N\mathbf{r}_i$ (which is $N$ times the coordinate of the center of mass) by taking its slope at long times,

$$D_c=\frac{1}{2dN}\lim_{t\to\infty}\frac{\mathrm{d}}{\mathrm{d}t}\left\langle\left\{\sum_{i=1}^{N}[\mathbf{r}_i(t)-\mathbf{r}_i(0)]\right\}^2\right\rangle. \tag{4}$$

The right hand side of Eq. (4) contains the correlations among *all* particles in the system at all instants of time. Depending on the particular randomization algorithm employed, correlations among different particles can be introduced. This in turn will give a collective diffusivity different from the self-diffusivity.

$D_c$ contains all the above mentioned time correlations relative to each single particle, plus the correlations between the displacements of each pair of particles at equal and different times, therefore we can express $D_c$ as[14]

$$D_c=D_s+D_{corr}, \tag{5}$$

where $D_{corr}$ contains all the time correlations between different particles. If, averaging over a long observation time, the positive and negative contributions to $D_{corr}$ cancel each other, then $D_{corr}$ becomes negligible so that $D_c$ converges to $D_s$ and we can say that the random walks of different particles are uncorrelated.

Finally the chemical diffusion coefficient $D_{chem}$ (sometimes reported as the *transport diffusivity*) measures the transport of mass and the decay of density fluctuations in the system, and it is related to the collective diffusivity by[15]

$$D_{chem}=\frac{\langle n\rangle}{\langle n^2\rangle-\langle n\rangle^2}D_c=\frac{\langle n\rangle}{\sigma^2}D_c, \tag{6}$$

where the quantity $\langle n\rangle/\sigma^2$ (i.e., the reciprocal of the reduced variance, see Paper I) is called the thermodynamic factor.

A useful quantity in the discussion of the diffusion properties of the model is the *accessibility* $\alpha_n$, defined for a cell of occupancy $n\geqslant 1$ as the equilibrium probability of an *exit site* to be occupied, divided by the occupancy (i.e., the number of particles in the cell) $n$. The probability $\alpha_n$ is independent of the loading $\langle n\rangle$ and measures the tendency of a particle to reach an exit site according to the number of particles which occupy the same host cell. It can be expressed as

$$\alpha_n=\frac{1}{n\nu}\sum_{n_{ex}=0}^{\nu}n_{ex}P^{eq}(n_{ex}|n), \tag{7}$$

where $P^{eq}(n_{ex}|n)$ has been defined in Eq. (5) of Paper I as the conditional probability of a cell to have $n_{ex}$ filled exit sites given that its occupancy is $n$. The average accessibility reads $\langle\alpha_n\rangle=\rho_{ex}/\langle n\rangle$. We plotted $\alpha_n$ versus $n$ for several temperatures in Fig. 1. Because the inner sites are the most binding, at finite $T$ the accessibility of the exit sites will increase with $n$.

At $T=300$ K, for low values of $n$ the probability of a particle to reach an exit site is very low and increases little

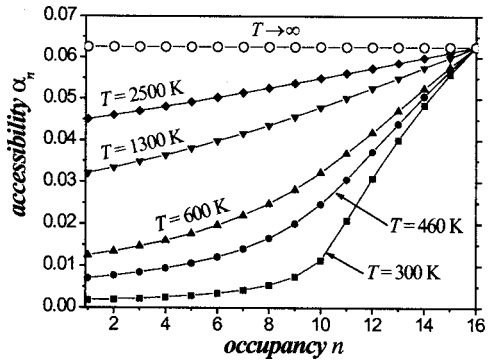


FIG. 1. Accessibility $\alpha_n$ vs the occupancy $n$ for various temperatures.

with increasing the occupancy. Instead, it increases rapidly when $n>(K-\nu)$ because in such cases at least $n-(K-\nu)$ exit sites must be occupied. In the limit of maximum occupancy $n=K$ the cell is saturated, and obviously we have $\alpha_n|_{n=K}=1/K$ independent of temperature.

Increasing the temperature, $\alpha_n$ becomes less occupancy sensitive and in the limit of $T\to\infty$ (which is equivalent to the case of $\varepsilon_{ex}=\varepsilon_{in}$) the accessibility is constant at $1/K$, because the sites are all equivalent.

The particular randomization operation adopted in this work (see Paper I) destroys the time correlations in the random walk of each single particle. This has two important consequences on the diffusivity.

- The self-diffusivity $D_s$ approximates well the self-diffusivity of an uncorrelated random walk $D_0$. This can be seen in the good overlapping of the profiles of $D_s$ and $D_0$ versus $\langle n\rangle$ for various temperatures, as shown in Fig. 2.
- As a consequence of this fact, if correlations *among different particles* exist they are *instantaneous*, that is, relative to the same time step. In our simulations we found $D_c\approx D_s$, therefore we say that under these conditions the correlations between the random walks of different particles are negligible and in Eq. (5) $D_{corr}\approx 0$. This can be seen in Fig. 3, where a good superposition of the self- and collective mean-squared displacements (MSD) is shown.

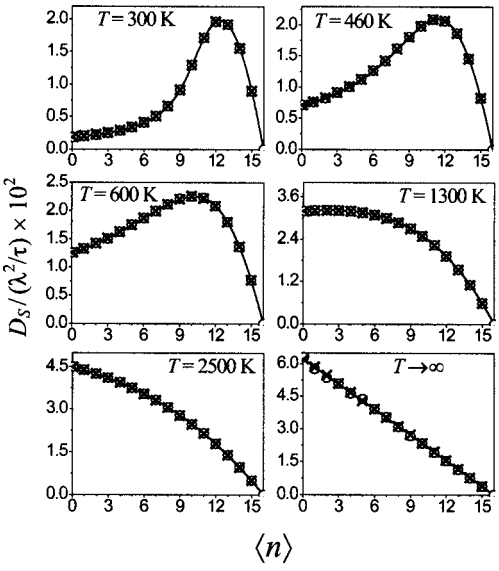


FIG. 2. Self-diffusivity (white circles) obtained from simulations at various temperatures, plotted together with $D_0$ obtained through direct measurements of the mean residence time [crosses, see Eq. (2)] and through Eq. (3) (solid line).

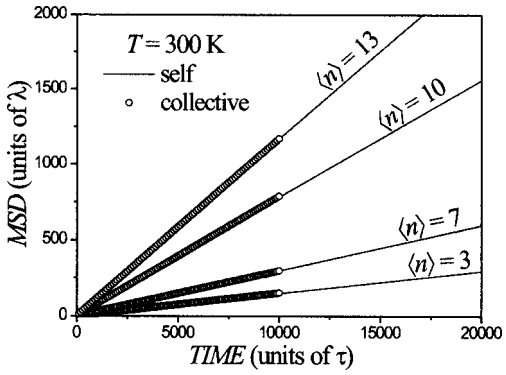


FIG. 3. Mean-squared displacement (MSD) of the self-coordinate $\mathbf{r}_i$ [see Eq. (1)] and of the collective coordinate $\Sigma_{i=1}^{N}\mathbf{r}_i$ [see Eq. (4)].

In Fig. 4 several profiles of (a) $D_s$, [inset of (b)] $D_c$, and (b) $D_{chem}$ are shown. We illustrate the obtained trends in the following.

### 1. Self-diffusivity

In Fig. 4(a) the behavior of $D_s$ versus loading is reported for various temperatures. Changes in temperature lead to different profiles of the self-diffusivity, corresponding to the I,

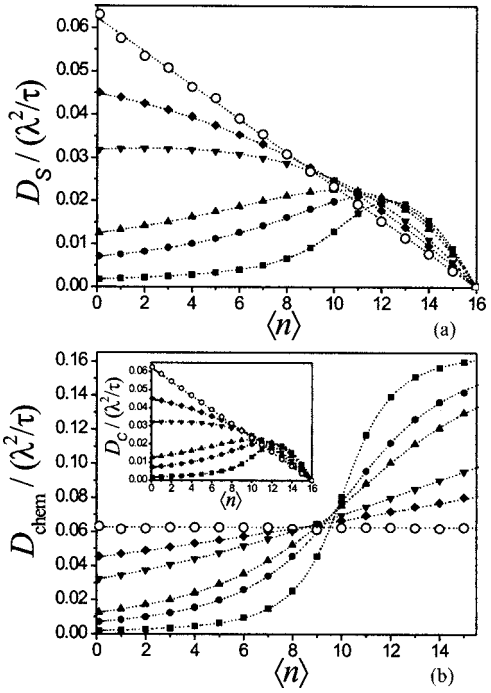


FIG. 4. (a) Self-diffusion coefficients for various loadings and temperatures, plotted together for a direct comparison. (b) Chemical diffusion coefficients obtained from the collective diffusivity $D_c$ (shown in the inset) and the thermodynamic factor using Eq. (6). $T=300$ K (squares), $T=460$ K (black circles), $T=600$ K (up triangles), $T=1300$ K (down triangles), $T=2500$ K (diamonds), and $T\to\infty$ K (white circles).

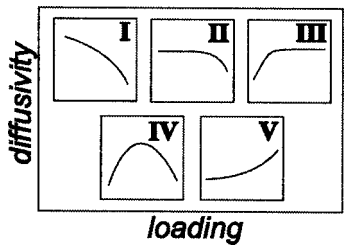


FIG. 5. The five different profiles of self-diffusivity vs loading observed by Kärger and Ruthven (Ref. 16).

II, IV, and V types observed by Kärger and Ruthven[16] (see Fig. 5) in the pulsed field gradient-NMR (PFG-NMR) measurements of intracrystalline self-diffusion coefficient depending on sorbate concentration.

We define as event 1 the event in which a particle reaches an exit site during randomization, and as event 2 the event in which two adjacent exit sites are simultaneously occupied during propagation. The probabilities of events 1 and 2 *increase* as the average accessibility $\langle \alpha_n \rangle$ of the exit sites increases. If by increasing the loading $\langle n \rangle$ they increase in different ways, then in general the resulting diffusivity trend will not be linear. With this in mind we proceed to describe the trends reported in Fig. 4(a) in detail.

(i) Let us consider first the self-diffusivity trend at $T=300$ K (black squares). From low to intermediate loading the curve shows the increasinglike behavior of type V, as reproduced by the model of Tunca and Ford,[17] because in this range of loadings the probability of event 1 increases more rapidly than the probability of event 2. Further increases of $\langle n \rangle$ will cause the diffusivity $D_s$ to increase until it reaches a maximum. At this point, the probabilities of events 1 and 2 are balanced: if we remove a small number of particles from the system the diffusivity will decrease due to a decrease of the probability of event 1; instead if we add a few particles the diffusivity will decrease because the average accessibility will become large enough to enhance the probability of event 2. Therefore, at intermediate-high loadings the diffusivity trend is of type IV ($D_s$ reaches a maximum and then decreases to zero). It should be noted that at $T=300$ K the behavior of $D_s$ versus $\langle n \rangle$ is qualitatively analogous to the trend obtained by us[18] and by Dubbeldam *et al.*[19] in molecular dynamics (MD) simulations of diffusion of methane in ZK4, and by Coppens and Iyengar[8] through dynamic Monte Carlo simulations of diffusion on a lattice with multiple types of sites.

(ii) The same considerations are valid for the self-diffusivity trends at $T=460$ and 600 K. Since the self-diffusion is ruled by event 1 at low loadings, and by event 2 at high loadings, for a fixed value of $\langle n \rangle$ an increase of the temperature will cause $D_s$ to increase considerably if $\langle n \rangle$ is low, while if $\langle n \rangle$ is high then $D_s$ will slightly decrease. In order to see a more detailed picture of the effect of the temperature on the diffusivity at constant loading, in Fig. 6 curves of diffusivity versus temperature are shown for $\langle n \rangle = 5$ and 13 (the loading which corresponds to the maximum diffusivity falls between these two loadings). Not only the response of $D_s$ to an increase of temperature is opposite from low to high loadings, but one can also see from the trends of Fig. 4(a) and from the diffusivity scales of Fig. 6 that the $D_s$ becomes less temperature sensitive when the system goes toward saturation, a situation at which the properties of the model become independent of temperature.

(iii) Further increases of temperature will change the diffusion profile. From $T=600$ K to $T=2500$ K the trends change from the type discussed before to the type I of Fig. 5, passing through the type II at $T=1300$ K, where the probabilities of events 1 and 2 are balanced for low loadings. At high temperature, say $T=2500$ K, the system behaves in a way very similar to the case of $T \to \infty$, at which $D_s$ decreases linearly with $\langle n \rangle$ because the sites are all equivalent, so that the accessibility is constant with $n$ (see Fig. 1) and the only effect controlling the migration process is mutual exclusion.

The diffusivity of type III is proper for a situation in which the balance between the probability of event 1 and the

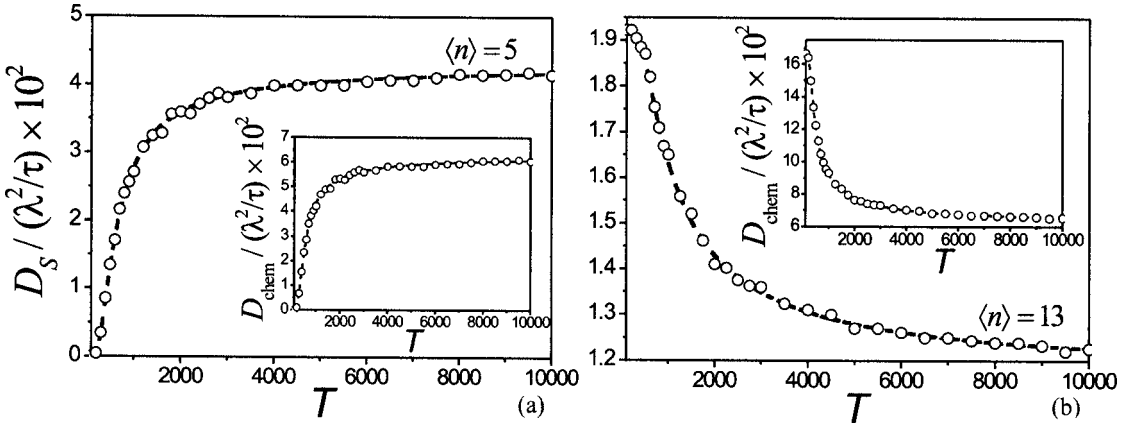


FIG. 6. Self-diffusivity $D_s$ and collective diffusivity $D_c$ (insets) vs the absolute temperature $T$ from $T=100$ K to $T=10\,000$ K. In (a) the loading is $\langle n \rangle = 5$ and in (b) it is $\langle n \rangle = 13$ (see text for details).

probability of event 2 persists for a loading interval around the loading of highest self-diffusivity. This diffusive behavior cannot be reproduced if $\varepsilon_{ex}, \varepsilon_{in}$ are held fixed. In order to provide the aforementioned balance which gives a $D_s$ trend of type III, one has to refine on the model in such a way to allow the introduction of an explicit dependence of the energy parameters on some local observables (e.g., the occupancy $n$), and then model this dependence to obtain the requested balance. On the other hand, this choice is reasonable since in real systems it is not uncommon for the energy of adsorption sites to be dependent on whether the neighboring sites are occupied,[20] and in principle this situation can be reproduced introducing occupancy-dependent adsorption energies, treated as adjustable parameters or obtained by means of a coarse graining of the interactions in a cell with a detailed arrangement of the adsorption sites.

One can see by direct comparison that the $D_s$ trends presented in Fig. 4(a) of this work are similar to the trends found by Bhide *et al.* (see Fig. 5 of Ref. 12) in the study of diffusion of *interacting* particles in a lattice with two nonequivalent sites, although these two models are quite different. Indeed, traditional Monte Carlo lattice gases are used to study the random walk of particles between neighboring positions in a fully detailed lattice of adsorption sites; on the contrary in our model the diffusion process is a random walk of particles *from cell to cell*, where each cell contains a number of adsorption sites without a fully defined spatial arrangement. Even working with noninteracting particles and neglecting the intracell motion time scale, the distinction between exit and inner sites is sufficient to reproduce an effect of confinement, giving rise to $D_s$ profiles which are typical of confined systems. Moreover the LGCA algorithm, with its parallel nature, is easier to implement in a parallel machine than a traditional kinetic Monte Carlo procedure.

#### 2. Chemical diffusion coefficient

The chemical diffusion coefficient $D_{chem}$ [see Eq. (6) and Fig. 4(b)] is given by the product of the *collective diffusivity* $D_c$ [see Eq. (4) and the inset of Fig. 4(b); in our case $D_c \approx D_s$] times the *thermodynamic factor* (defined as the reciprocal of the reduced variance; see Paper I and Ref. 9 for further details).

At infinite temperature the reduced variance (see Paper I) and $D_c$ respond to an increase of density exactly in the same way (i.e., they are both linearly decreasing with $\langle n \rangle$). This results in a $D_{chem}$ constant with loading.

This balance between fluctuations and diffusive properties is broken when the difference in binding ability of the two types of site becomes non-negligible. Lowerings of temperature will reduce the density fluctuations, and the $D_{chem}$ profile will show two distinct diffusive regimes:[21] low diffusivity for low loadings and high diffusivity for high loadings. Similarly to the case of $D_s$, increasing the temperature the difference between $\beta\varepsilon_{ex}$ and $\beta\varepsilon_{in}$ will become less relevant and $D_{chem}$ will change less with temperature. For high temperatures $D_{chem}$ will increase almost linearly with $\langle n \rangle$, with a slope decreasing with $T$ until it reaches the above discussed profile at $T \to \infty$.

At constant loading the trend of $D_{chem}$ with respect to $T$ is similar to $D_s$ (see Fig. 6). The difference is that, while $D_s$ is very temperature sensitive at low loadings but less sensitive at high loadings, $D_{chem}$ is very temperature sensitive for both low and high loadings.

The use of the randomization rule described in Paper I allows the random walks of the particles to be treated, with a good approximation, as independent Markov processes. Time correlations in the self-motion and between different particles are so weak that all of the diffusivities $D_s$, $D_c$, and $D_{chem}$ scale linearly with $\kappa_0$.

### B. Local density

To supplement the picture of the migration process given in the previous section, we study the change in time of the local density. We explore the following:

- the *mean lifetime* of the occupancy $n$, defined (in units of time steps) as the average number of consecutive time steps during which a cell persists in the occupancy $n$;
- the time-autocorrelation function of the fluctuations of the occupation number,[22]

$$C(t) = \langle \delta n(0)\, \delta n(t) \rangle, \tag{8}$$

where $\delta n(t) = n(t) - \langle n \rangle$. Because $C(t)$ with $\kappa_0 = 1$ relaxes very fast toward equilibrium, in order to clearly see the details of the relaxation process in this section we report results for $\kappa_0 = 0.1$. Indeed the effect of this choice is a homogeneous slowing down of the intercell migration process which does not influence the equilibrium properties of the lattice.

#### 1. Mean lifetime

Particles going in and out of a cell will vary the cell occupancy.

In Fig. 7 curves of the mean lifetime (MLT) are shown for a relatively low temperature, $T = 300$ K, and for infinite temperature. For each loading, data are plotted only for the most probable occupancies (i.e., we choose the occupancies $n$ such that $f^{eq}(n) > 10^{-3}$).

- Observing the behavior of this function for $T = 300$ K (Fig. 7), we note how a non-negligible difference between $\beta\varepsilon_{ex}$ and $\beta\varepsilon_{in}$ introduces a separation in the mean lifetime of different occupancies, causing the curves to cover several orders of magnitude on the time axis. (i) For low and intermediate loadings, the less filled cells live longer because they host all or almost all of the particles in the inner sites, therefore the particle transfers are little frequent and so the variations of the lowest occupancies. (ii) If the loading increases, then $\langle \alpha_n \rangle$ will increase, therefore the transfers will become more frequent and this will reduce the MLT of all the occupancies. Moreover, the mean lifetimes will be less sensitive to $n$. It is worth noting that this is the same kind of behavior shown by the MLT of the occupancies in the $\alpha$ cages in MD simulations of diffusion of methane in ZK4 (see Fig. 6 of Ref. 23). This confirms that our

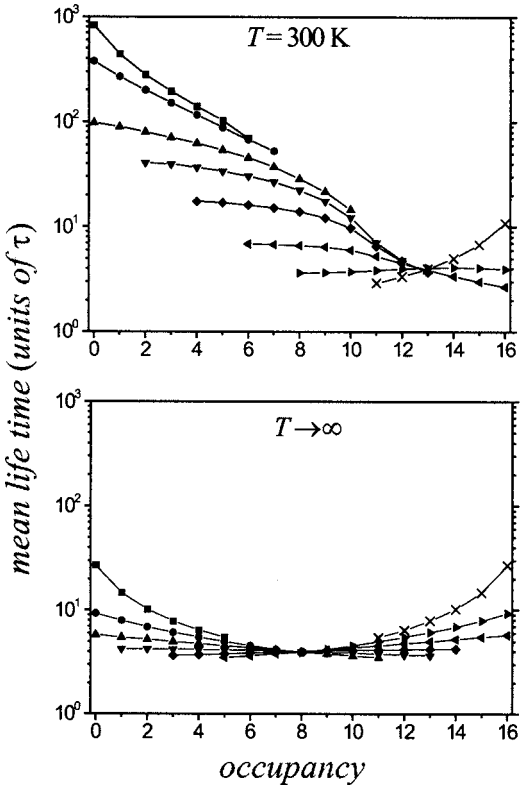


FIG. 7. Curves of the mean lifetime of a cell as a function of the occupancy at $T=300$ K and $T\to\infty$. Each curve corresponds to a particular loading. $\langle n\rangle=1$ (squares), $\langle n\rangle=3$ (circles), $\langle n\rangle=5$ (up triangles), $\langle n\rangle=7$ (down triangles), $\langle n\rangle=9$ (diamond), $\langle n\rangle=11$ (left triangles), $\langle n\rangle=13$ (right triangles), and $\langle n\rangle=15$ (crosses). For each loading, data are plotted only for the most probable occupancies (i.e., the occupancies appearing with a probability $>10^{-3}$).

LGCA approach effectively captures the essential features of the process of diffusion in zeolites. (iii) For the highest loadings (e.g., $\langle n\rangle=15$ in Fig. 7), the more filled cells will release particles *slightly* more slowly because almost all of the exit sites will be occupied, therefore the mean lifetimes of the most occupied cells will be slightly longer.

- The separation in MLT of cells with different occupancies becomes less evident by increasing the temperature. In the limit of $T\to\infty$ (see Fig. 7) the sites are all equivalent, therefore the mean lifetimes are all of the same order of magnitude, and the MLT curves are more symmetrical when compared to the case of diffusion in the presence of the energy effects discussed in the previous point.

### 2. Time autocorrelation of density fluctuations

The study of the function $C(t)$ defined in Eq. (8) provides informations about how the local density fluctuations relax in time toward equilibrium.

In Figs. 8(a)–8(c) the normalized time-autocorrelation function $C(t)/C(0)$ is reported. The best fit of $C(t)/C(0)$ is provided by a double exponential function

$$C(t)/C(0)\approx A_1 e^{-t'/\tau_1}+A_2 e^{-t'/\tau_2}, \tag{9}$$

where $t'=t/\tau$ is the time expressed in units of time steps, while $A_{1,2}$ and $\tau_{1,2}$ are fitting parameters. As can be seen in Fig. 8(c), a simple exponential decay is inappropriate to fit the simulation data.

The relaxation of the density autocorrelation is reported at low temperature ($T=300$ K) in Fig. 8(a) and at very high temperature ($T\to\infty$) in Fig. 8(b). If the temperature is low, the relaxation is different for different loadings; in particular, at high $\langle n\rangle$ the function $C(t)/C(0)$ goes to zero more rapidly than at low $\langle n\rangle$. This feature is also exhibited by the autocorrelation of density fluctuations computed in MD simulations (see Fig. 8 of Ref. 23). When the temperature is increased, the relaxations at different loadings become similar. This can be seen from Fig. 9, where the quantity $1/\tau_{\mathrm{rel}}$ is shown for various loadings and temperatures. $\tau_{\mathrm{rel}}$ is the instantaneous relaxation time, defined as the time employed by the fit of $C(t)/C(0)$ to reach $1/e$ of its initial value. As the temperature becomes very large, the relaxation becomes independent of temperature, as well as the chemical diffusion coefficient. This behavior supports the observations we have made in the previous section about the separation of the mean lifetimes: the local density relaxes in time in a way dependent on the degree of inhomogeneity of the lattice, which becomes important at low temperature.

As can be seen from the proportionality between $1/\tau_{\mathrm{rel}}$ and $D_{\mathrm{chem}}$ shown in Fig. 9, the decay of the density fluctuations controls the transport of density in the lattice. It should be noted that the behavior of the dynamical property $C(t)$ is strictly connected with the particular form of the evolution algorithm employed. Even if different evolution algorithms,

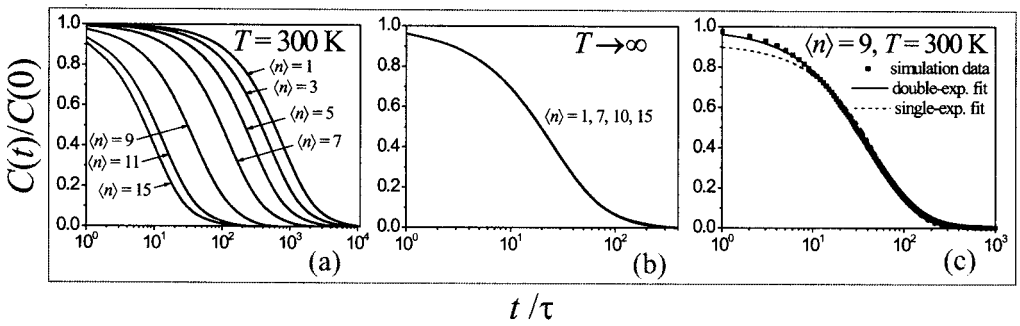


FIG. 8. Normalized time-autocorrelation function $C(t)/C(0)$ for various loadings at (a) $T=300$ K and (b) $T\to\infty$. In (c), $C(t)/C(0)$ for $\langle n\rangle=9$ at $T=300$ K is shown: simulation data, single exponential fit, and double exponential fit.

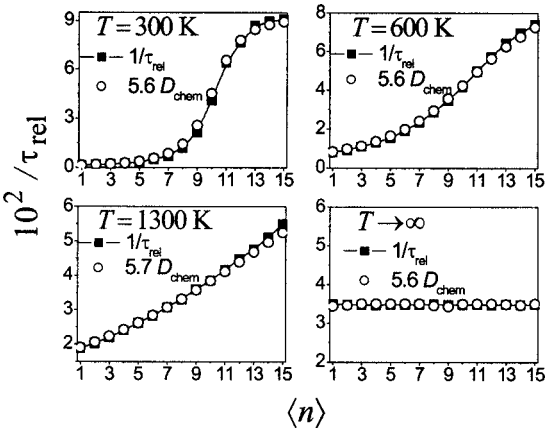


FIG. 9. Inverse of the instantaneous relaxation time $\tau_{\mathrm{rel}}$ obtained through the double exponential fit of $C(t)/C(0)$, compared with the chemical diffusion coefficient $D_{\mathrm{chem}}$.

provided they satisfy the microscopic reversibility, sample the same points in the configuration space, the way the density fluctuations decay toward equilibrium can be different from rule to rule. A particular form of the probabilities $R(\mathrm{s}\rightarrow \mathrm{s}^R)$ and $p^P$ in the randomization and propagation algorithms can be preferred to another one on the basis of the likeness of the obtained relaxation with the relaxation of the physical process the model attempts to mimic. Therefore, further simulations and analyses are required to study the behavior of $C(t)$ with different evolution rules; this will be the subject of a forthcoming paper.

## III. CONCLUSIONS

In this paper we gave a reductionistic description of a zeolitic framework. It is presented as a static network of cells (cages) each other connected by a fixed number of links according to a cubic symmetry. Evolution rules were *ad hoc* introduced to simulate the diffusion of particles in tight confinement: each cell can host a limited number of particles, and a parallel rule connects neighboring cells in such a way that two adjacent cells can exchange at most one particle in one time step. The low temperature enhances the difference in probability of occupation of two different kinds of site inside of each cell. We analyzed the coverage-temperature dependence of self-, collective, and chemical diffusivities, mean lifetime of a cell in a particular occupancy, and the decay of local density fluctuations. The choice of an evolution rule destroying the time correlations in the particle migration process causes the self- and the collective diffusivities to be similar to the self-diffusivity of an uncorrelated random walk. At very high temperature the lattice is homogeneous, then the diffusion is governed only by mutual exclusion. Therefore self- and collective diffusivities decrease linearly with loading and different occupancies show mean lifetimes of the same order of magnitude, while chemical diffusion coefficient and time relaxation of the local density fluctuations are independent of loading. Lowering the temperature, mutual exclusion, and energy effects add together to give a nontrivial loading dependence of diffusivities, mean lifetimes, and local density relaxation. In particular, self-diffusivitiy profiles are in agreement to four of the five types of self-diffusivity observed by Kärger and Ruthven[16] in PFG-NMR experiments, and for low temperatures the profiles of self-diffusion, mean lifetimes, and relaxation times of density fluctuations are in qualitative agreement with MD simulations of methane in ZK4.[18,19,23]

In conclusion our model captures effectively the phenomenology of the diffusion in tight confinement of weakly interacting species by means of a cellular structure evolving in time with a fast, parallel rule allowing to study systems for space-time scales larger than conventional simulations. Presently we are working to extend the results discussed herein to take into account the action of local guest-guest interactions that we will address in a forthcoming publication.[24] Further study is essential to find out how widely applicable the LGCA illustrated in these papers is to transport problems in other host-guest systems with a topology different from the simple cubic presented here.

We note that our LGCA is quite general and can be easily extended to other research areas where the considered system can be represented as a network of interacting structured cells that can exchange information according to a set of local rules.

## ACKNOWLEDGMENTS

This work has been carried out with financial support provided by Italian Ministero dell'Istruzione, dell'Università e della Ricerca, by Università degli Studi di Sassari, by INSTM, and by the COSMOLAB Consortium (CYBERSAR Supercomputing Research Project).

## APPENDIX: IDEAL DIFFUSIVITY

In order to compute the inverse mean residence time $\tau_{\mathrm{mrt}}^{-1}$, which (since $\tau_{\mathrm{mrt}}$ is expressed in units of time step) is the probability of a particle to migrate from a cell to a neighboring one during one time step, we have to find the following:

(i) the probability of a particle to reach any one of the $\nu$ exit sites in its host cell, which reads $\nu\rho_{\mathrm{ex}}/\langle n\rangle$;

(ii) the conditional probability of a particle to be able to migrate to the corresponding neighboring cell, given that it reached an exit site during randomization; this is the probability of the adjacent exit site to be unoccupied times the probability of the jumping particle to overcome the barrier for intercell migration, i.e., $(1-\rho_{\mathrm{ex}})\kappa_0 A e^{-\beta\varepsilon_{\mathrm{ex}}}$ where $\kappa_0$ and $A$ are constant parameters (see Paper I).

Therefore

$$\tau_{\mathrm{mrt}}^{-1}=\frac{\nu\rho_{\mathrm{ex}}}{\langle n\rangle}(1-\rho_{\mathrm{ex}})\kappa_0 A e^{-\beta\varepsilon_{\mathrm{ex}}}, \tag{A1}$$

which can be introduced in Eq. (2) to obtain Eq. (3).

[1] S. M. Auerbach, F. Jousse, and D. P. Vercauteren, in *Computer Modelling of Microporous and Mesoporous Materials*, edited by C. R. A. Catlow, R. A. van Santen, and B. Smit (Elsevier, Amsterdam, 2004), pp. 49–108.
[2] E. S. Fois, A. Gamba, C. Medici, and G. Tabacchi, ChemPhysChem **6**, 1917 (2005).
[3] P. Demontis, J. Gulín-González, and G. B. Suffritti, J. Phys. Chem. B

**110**, 7513 (2006).
[4] C. Alba-Simionesco, B. Coasne, G. Dosseh, G. Dudziak, K. E. Gubbins, R. Radhakrishnan, and M. Sliwinska-Bartkowiak, J. Phys.: Condens. Matter **18**, R15 (2006).
[5] C. Tunca and D. Ford, J. Chem. Phys. **111**, 2751 (1999); J. Phys. Chem. B **106**, 10982 (2002).
[6] C. Saravanan, F. Jousse, and S. M. Auerbach, Phys. Rev. Lett. **80**, 5754 (1998).
[7] M.-O. Coppens, A. T. Bell, and A. K. Chakraborty, Chem. Eng. Sci. **53**, 2053 (1998).
[8] M.-O. Coppens and V. Iyengar, Nanotechnology **16**, S442 (2005).
[9] P. Demontis, F. G. Pazzona, and G. B. Suffritti, J. Phys. Chem. B **110**, 13554 (2006).
[10] S. Fritzsche, R. Haberlandt, J. Kärger, H. Pfeifer, and M. Wolfsberg, Chem. Phys. Lett. **198**, 283 (1990).
[11] S. Y. Bhide and S. Yashonath, J. Chem. Phys. **111**, 1658 (1999).
[12] S. Y. Bhide and S. Yashonath, J. Phys. Chem. B **104**, 2607 (2000).
[13] F. R. Keil, R. Krishna, and M.-O. Coppens, Rev. Chem. Eng. **16**, 71 (2000).
[14] R. Gomer, Rep. Prog. Phys. **53**, 917 (1990).
[15] C. Uebing and R. Gomer, J. Chem. Phys. **95**, 7626 (1991).
[16] J. Kärger and D. M. Ruthven, *Diffusion in Zeolites and Other Microporous Materials* (Wiley, New York, 1992).
[17] C. Tunca and D. Ford, Chem. Eng. Sci. **58**, 3373 (2003).
[18] P. Demontis and G. B. Suffritti, J. Phys. Chem. B **101**, 5789 (1997).
[19] D. Dubbeldam, E. Beerdsen, T. J. H. Vlugt, and B. Smit, J. Chem. Phys. **122**, 224712 (2005).
[20] E. Beerdsen, D. Dubbeldam, and B. Smit, J. Phys. Chem. B **110**, 22754 (2006).
[21] Z. Chvoj, H. Conrad, V. Cháb, M. Ondrejcek, and A. M. Bradshaw, Surf. Sci. **329**, 121 (1995); Z. Chvoj, H. Conard, and V. Cháb, *ibid.* **376**, 205 (1997).
[22] D. Chandler, *Introduction to Modern Statistical Mechanics* (Oxford University Press, New York, 1987).
[23] P. Demontis, L. Fenu, and G. B. Suffritti, J. Phys. Chem. B **109**, 18081 (2005).
[24] P. Demontis, F. G. Pazzona, and G. B. Suffritti, J. Chem. Phys. **126**, 194709 (2007), preceding paper.